Pharmaceutical Sciences, 2024, 30(2), 262-273
doi:10.34172/PS.2024.4
https://ps.tbzmed.ac.ir/

Research Article

Biogenic Zinc Oxide Nanoparticles Attenuate Acute Lymphoblastic Leukemia Cell Proliferation through Oxidative Stress and DNA Damage

Sujatha Venugopal[1,2*], Venkatesan Alagesan[1], Sancharan Acharya[3], Thirunavukkarasu Chinnasamy[3]

[1]*Department of Chemistry, Pondicherry University, Puducherry-605014, India.*
[2]*Department of Chemistry, Periyar University, Salem 636011, Tamil Nadu, India.*
[3]*Department of Biochemistry and Molecular Biology, Pondicherry University, Puducherry-605014, India.*

Article Info

Article History:
Received: 13 Nov 2023
Accepted: 2 Feb 2024
ePublished: 28 Feb 2024

Keywords:
-Acute lymphoblastic leukemia
-DNA damage
-*Diospyros montana*
-MOLT3
-Oxidative stress
-Zinc oxide nanoparticles

Abstract

Background: The most prevalent pediatric cancer is acute lymphoblastic leukemia (ALL). It is exceedingly challenging to treat recurrent diseases, and there aren't many new medications available for children with disease resistance. The size-dependent anticancer effect of zinc oxide nanoparticles (ZnONPs) on T-cell acute lymphoblastic leukemia (T-ALL) cell line MOLT 3 is the central theme of this study.

Methods: The leaf and bark extracts of *Diospyros montana* were subjected to nanoparticle (NPs) synthesis and characterized analytically to acquire ZnONPs. The ZnONPs were characterized using UV-Vis spectra, DLS, XRD, EDX, SEM, and TEM analysis. Then the ZnONPs were separated into two groups having <50 nm and 50-100 nm NPs sizes. In addition, MTT assay, dual staining, autophagy, DNA damage, and oxidative damage measurement were done to find out the anti-cancer effect of the ZnONPs on MOLT 3 cells.

Results: The ZnONPs exhibited a size-dependent anticancer effect against MOLT 3 cells. The IC_{50} of ZnONPs of < 50 nm was found to be ~75 µg/mL while the IC_{50} of ZnONPs of 50-100 nm size was found to be ~102 µg/mL. Treatment with ZnONPs of <50 nm size decreased mitochondrial membrane potential, more than that with 50-100 nm ZnONPs. On the other hand, autophagy was found to be more prevalent in 50-100 nm treated ZnONPs when compared with < 50 nm size. However, treatment with both sizes of ZnONPs reduced cell proliferation markers such as ki67 positive cells while increasing 8-OHG and HDCF-DA positive cells.

Conclusion: The obtained results portrayed that different-sized ZnONPs induce different modes of T-ALL cell death. Small-sized ZnONPs revealed higher efficacy, highlighting the size-dependent property. Further, this finding denotes that ZnONPs could be an effective anticancer agent against dreadful diseases like T-ALL, warranting further investigation.

Introduction

Acute lymphoblastic leukemia (ALL) is an extremely heterogeneous disease. Immature lymphoid cell growth and accumulation in the bone marrow, peripheral blood, lymphoid organs, and other extra-nodal locations are hallmarks of ALL. The World Health Organization (WHO) defines ALL as either B-cell ALL (B-ALL) or T-cell ALL (T-ALL).[1] Mature or precursor T-cells are equal contributors to T-cell malignancies, which may occur in children (below 18 years) or young adults (19-26 years). However, they are generally clustered into two classes namely (i) T-ALL & T-cell lymphoblastic lymphoma (T-LBL), and (ii) Peripheral T-cell lymphomas (PTCL). The most common T-cell malignancy in children is T-ALL. This type of T-cell malignancy accounts for around 15% of all pediatric ALL cases[2] and of all pediatric cases of non-Hodgkin lymphoma. T-ALL needs more attention because of its greater propensity to invade extra-lymphatic spaces, including the central nervous system.

Different types of T-cell leukemia are distinguished based on the level of bone marrow participation. In T-ALL, bone marrow contribution is more, which is 25%, however it may still exist with lymph node participation. On the other hand, other T-cell leukemia have 5-25% bone marrow contribution, which is much lower than that of T-ALL.[3,4] Irrespective of different T-ALL origins, the treatment method is coordinated with other T-cell leukemia such as T-LBL. Different modes of treatment such as radiation, stem cell transplantation, etc, in T-ALL, show better outcomes, but relapse patients' cure rates are lower than 30%,[5] and outcomes for relapsed T-LBL are even worse.[6]

The three phases of the treatment strategy used to manage ALL patients are remission induction, consolidation, and long-term maintenance, as well as central nervous system

*Corresponding Author: Sujatha Venugopala, E-mail: sujathav.che@pondiuni.edu.in & sujatha888@periyaruniversity.ac.in

prophylaxis. Standard chemotherapy is the frontline treatment for induction therapy. In all three strategies, chemotherapy or targeted drug candidates can be used as such or in combination with chemotherapy.[7] At present, 80-90% survival rates in children and adolescents up to 19 years were achieved because of the dedicated contributions of different researchers over the past 40 years.[8-10] However, the long-term remission is around 30-40% in adult patients.[8,11,12] Recently, endogenous T cell-mediated immunotherapies have been developed as a novel approach to manage ALL patients and evade cancer drug resistance.[13] Therefore, innovative treatment agents are timely in need to avoid relapse in patients and also to manage adolescents and children with T-ALL. Hence, researchers are exploring deeply effective compounds and innovative treatments free of these problems.

Imbibed multifunctional properties of nanoparticles (NPs) have been significantly explored in the pharmacological field.[14-16] These pharmacological applications could be hindered if NPs were contaminated with even traces of toxic substances. NPs synthesized through chemical processes cause undesirable effects when subjected to biological applications. This disadvantage could be due to the constituents used in the synthesis of NPs. Generally, NPs synthesized by plant extract are reported to be non-toxic and hazard-free, further, this procedure has been proven to be eco-friendly, and in addition, it is a one-step process.[17-19] Because of their surface-to-volume ratios, the NPs display different physical and chemical properties. Active phytochemicals present in medicinal plants were reported to suppress the growth and advancement of tumors in diseased patients.[20] Further, different phytochemicals are responsible for the development of NPs, when plant extracts are used to manufacture NPs. Trace-level attachments of these phytoconstituents to NPs are not ruled out. As raw phytochemical extracts themselves could diminish the progression of cancer cells,[21] the attachment of these compounds to NPs will have an added advantage, when NPs are aimed for an anticancer effect. Based on the revival of ancient medicine, researchers are now focusing more on plant-derived green NPs for cancer treatment because they require less time and money. Furthermore, green synthesized NPs are conjugated to make targeted delivery, which is also less expensive when compared to conventional synthetic compounds.[22,23]

Diospyros montana Roxb. (*D. montana*) is one of the medicinally important plants that possess effective pharmacological properties and therapeutic value in traditional systems of medicine.[24] It is found in deciduous forests and is broadly spread around India. *D. montana* contains multiple bioactive constituents such as tannins, alkaloids, flavonoids, terpenoids, etc.[24-26] Reports reveal its imperatively potent pharmacological activities and its use, in the treatment of snake-bites, ulcers, hypersensitivity, and cough.[27,28] Recently, *D. montana* has been used in the biosynthesis of silver and selenium NPs.[27,29]

Zinc oxide nanoparticles (ZnONPs) are synthesized using nanotechnology and are widely used in different disciplines such as beauty products, biosensors, optical devices, ceramics, used in solar cells, and drug delivery.[30-32] Reports indicate that cancerous cells are killed by ZnONPs, whereas normal cells remain unaffected in the same concentration.[33,34] Literature indicates that the cell response to ZnONPs is dynamic. Premanathan *et al.*[35] stated that the final effective concentration depends on multiple challenging factors which include, intersecting signals in the microenvironment of cancer cells. Further, they have reported that ZnONPs were more hazardous to HL60 cancer cells than to normal human peripheral blood mononuclear cells. By green synthesized ZnONPs, different investigators have shown their anticancer effect on several *in vitro* and *in vivo* cancer cells/models. However, to our knowledge, there is no literature on the effect of different-sized ZnONPs on T-ALL cells. In the context of the above discussion, the current investigation aims to synthesize ZnONPs by green route, characterize, and differentiate their size distribution, and evaluate their anti-leukemic properties size dependently along with the potential mechanism of action.

Materials and methods

Chemicals

$(Zn(NO_3)_2).6H_2O$ of 99% purity was obtained from Sigma-Aldrich, India. 10x phosphate buffered saline (PBS) and dimethyl sulfoxide (DMSO), were procured from Himedia. All other essential chemicals were obtained from Himedia companies and Merck India Private Limited which were of high purity and analytical grade. Deionized water was used for all the experiments.

Plant collection

D. montana (F. Ebenaceae) were collected and authenticated as explained in Kokila *et al.*,[27] however, the current batch obtained via document no: BSI/SRC/21/11/2019/Tech/1791. Fresh healthy leaves and bark were handpicked, dusted, and washed thoroughly with distilled water. Leaves and barks were shade-dried and made into a fine powder using a blender. Methanol leaf extracts (MeLE) and methanol bark extracts (MeBE) were prepared by Soxhlet extraction (72 hours of consecutive running) with 200g of plant sample and 300 mL of methanol until the solution became colorless. Whatman No.1 paper was used to filter the extract to obtain clean and clear MeLE and MeBE. The concentrated crude extracts were stored at 4° C for further experiments.

Green synthesis of ZnONPs

10 mL of MeLE and MeBE were added with 100 mL of deionized water separately and heated at 50-60° C with constant stirring for about 30 mins to obtain a homogeneous solution. The various concentrations (0.5-10 mM) of metal precursor $(Zn(NO_3)_2).6H_2O$ were added to the methanol homogeneous solution of MeLE and MeBE separately. Solutions were stirred continuously

for 4-6 hours at a temperatureof 80° C. By centrifuging at 10000 rpm for 15 mins the formed precipitate was separated. Then the precipitate was allowed to dry at room temperature (RT) ranging between 25-27° C. The powder material was calcinated in a muffle furnace at 400° C for 1 hour. ZnONPs were obtained as a fine powder from the MeLE (MeLE-ZnONPs) and MeBE (MeBE-ZnONPs). They were stored in an airtight container forfurther experiments.

Characterization techniques

The synthesized MeLE-ZnONPs and MeBE-ZnONPs were subjected to various spectral studies such as UV-Vis spectroscopy, dynamic light scattering (DLS), Fourier transforms infrared (FT-IR) spectroscopy, X-ray diffraction (XRD), scanning electron microscope (SEM), energy-dispersive X-ray spectroscopy (EDX) and transmission electron microscopy (TEM) analysis. The synthesized ZnONPs absorption maxima were identified by scanning the nanoparticle at 200-800 nm range at a scanning speed of 480 nm/min in a UV-VIS-NIR spectrophotometer (Shimadzu, Model-3600, North America). The active functional groups of MeLE-ZnONPs and MeBE-ZnONPs were examined by FT-IR spectroscopy (Thermo Nicolet, Model-6700, US) using about 2 mg of MeLE- ZnONPs and MeBE-ZnONPs with KBr pellets (100mg) that were read at the range of 400 to 4000 cm^{-1} wavelength with a resolution of 1 cm^{-1}. X-ray diffractometer (PAN analytical, The Netherlands) was used to study the crystalline nature, size, and purity of MeLE-ZnONPs and MeBE-ZnONPs. The source of X-ray was Cu-Kα radiation (λ =1.541 Å) and Scherrer's equation ($D \approx 0.9\lambda\beta\cos\theta$) was employed to detect the size of MeLE-ZnONPs and MeBE-ZnONPs. The average hydrodynamic size of MeLE-ZnONPs and MeBE-ZnONPs was analyzed by using the Malvern-Zetasizer instrument which was equipped with a 4mW He-Ne laser. Huang and Zhu[36] method was adopted to calculate the percent NPs production yield. The morphological characteristics of the MeLE-ZnONPs and MeBE-ZnONPs were observed under scanning electron microscopy (SEM, Hitachi, Model-S-3400N, USA) and High-resolution transmission electron microscopy (HRTEM, Tecnai G2 F30 S Twin, USA) analysis. The elemental composition of MeLE-ZnONPs and MeBE-ZnONPs was investigated using EDX analysis.

Separation of NPs using double-phase separation method

The separation of MeLE-ZnONPs was achieved by a double-phase separation method using chloroform, a hydrophobic organic solvent, and water.[37] Initially, this mixture was centrifuged at 10000 rpm for 10 mins. The additional excess solvent present in the supernatant was removed, and the pellet was re-suspended in water. Again, chloroform was added and was vortexed for 5-10 seconds. After whirling, the organic and aqueous phases separated immediately into two distinct phases showing a clear boundary of interface. In addition, the flakes which were then recognized to be MeLE-ZnONPs aggregates, were found to move across the separation instantly and settled at the bottom of the chloroform phase. The total settling of MeLE-ZnONPs occurred in around 30 minutes. Along with this, centrifugation was done to facilitate the settling and collection of two phases. A pipette was used to collect the water phase and the NPs pellets were washed. The collected chloroform phase from the bottom was rewashed with chloroform. Finally, this two-phase NPs pellet was dried and used for further analysis.

Anticancer activity

The human ALL cell line, MOLT-3 was obtained from NCCS Pune, India. The cells were cultured in RPMI 1640 medium supplemented with fetal bovine serum (10 % FBS), 2 mM L-glutamine 1.5 g/L sodium bicarbonate, 0.1 mM sodium pyruvate, and 0.1 mM non-essential amino acids. Cells were maintained at 37° C in a 100% humidified incubator equipped with 5 % CO_2.

Cell viability assay and dual staining

The cytotoxicity of ZnONPs was assessed in MOLT-3 cells (1×10^6 cells per well) treated with ZnONPs (5 to 160 µg/mL and incubated for 48 hours). The cytotoxicity of ZnONPs was evaluated as a percentage of cell viability using colorimetric 3-(4,5-dimethyl-2- thiazolyl)-2,5-diphenyl-2H-tetrazolium bromide (MTT) assay as previously described by Ezhuthupurakkal *et al.*[38] The cytotoxic IC_{50} values of ZnONPs were calculated using graphical method by curve fitting analysis. The dual ethidium bromide/ acridine orange (EtBr/AO) staining[38] was also performed to differentiate the normal live cells, apoptotic cells, and necrotic cells that validated the apoptosis process in the MOLT-3 cells.[39] In detail, 1 µL of EtBr/AO staining solution (100 µg/mL EtBr & 100 µg/mL AO) was added to the cell suspensions. Cell morphology was observed through an Olympus (CX 40) fluorescent microscope. Around 200 cells were counted in randomly selected areas for statistical analysis.

The mitochondrial membrane potential (MMP) resolved by JC-1 staining

The MOLT-3 cells (1×10^6) cells were treated with IC_{50} concentration of ZnONPs for 48 hours at 37° C, subsequently cells were incubated with JC-1 (Cayman Chemical Company, MI, USA) stain (1 µg/mL) with the nuclear stain DAPI (1 µg/mL) (4082S, Cell Signaling, Beverly, MA) for 30 mins at 37° C. MMP was determined through JC-1 staining as explained in Smiley *et al.*[40] After the incubation, the medium was discarded and the cells were washed with 1×PBS. Then, it was resuspended in 30–50 µL of PBS and the MMP was examined under the fluorescence microscope (Olympus CX 40). Further, fluorescence intensity was quantified by Image J software.

Detection of acidic vacuole by acridine orange (AO) staining

AO has been used as an autophagy detection probe. The

cells were treated with the IC_{50} concentration of ZnONPs for 48 hours, the medium was discarded and washed with PBS. Autophagy was examined through AO staining as explained in Damas-souza.[41] Further, AO (5 µg/mL) was added, after 15 mins incubation, washed with PBS, and images were taken with a fluorescence microscope.

Immunofluorescence staining

The MOLT-3 cells were treated with IC_{50} concentration of ZnONPs for 48 hours after the cells were fixed with 4% formaldehyde and permeabilized with 0.1% Triton X-100, further, the experiment was carried out as mentioned in Ezhuthupurkkal *et al.*[38] For 8-OHdG, cells were treated with 25 ng/mL RNase A for 1 hour at 37° C, then 4 mol/L HCl was used for hydrolyzation for 7 mins, further neutralized with 50 mmol/L Tris base for 2 mins. Subsequently, cells were blocked with 1% bovine serum albumin (BSA) and incubated with anti-8OHdG antibody (1:1000; GTX41980; GeneTex, Irvine, CA), and Ki-67 (1:200, BD pharmingen™, USA) at 4° C for overnight with shaking. After rinsing with PBS, the cells were incubated with secondary antibody IgG, peroxidase-conjugated goat anti-mouse (A3682; Sigma) for 1 hour, and DAPI for 10 mins. Images were taken with a fluorescence microscope.

Cytosolic ROS generation evaluated by HDCF-DA staining

2, 7- dichlorodihydrofluorescein diacetate (HDCF-DA) is a sensitive, fastest, easiest, and commonly employed method for the detection of intracellular reactive oxygen species (ROS). MOLT-3 (1×10^5) cells were treated with IC_{50} concentration of ZnONPs and the experiment was carried out as explained in Wojtala *et al.*[42] At the end of the experimental period, cells were incubated with HDCF-DA for 10 mins. After the incubation, the cells were washed with PBS, resuspended in 30–50 µL of PBS containing 20 µg/mL bis-benzimide trihydrochloride (Hoechst 33258), and incubated at room temperature for 15 mins. The images were captured by a fluorescence microscope Olympus CX 40. The fluorescence intensity was measured using Image J software.

Statistical analyses

Results obtained in triplicates were presented as mean ± SD (standard deviation). Variances were considered to be significant at $P\leq 0.05$ against control and ZnONPs treated groups. For statistical analyses, ANOVA and Tukey's multiple tests were used. Origin software was used for the analysis of the data.

Results

Synthesis and characterization of ZnONPs

ZnONPs were developed (Figure S1) from MeLE and MeBE. The color change indicated the development of NPs. The formation of ZnONPs was preliminarily confirmed by UV-visible spectra as shown in Figure S2. MeLE alone showed (Figure S2a) absorbance at 259 nm and 379 nm. Likewise, the MeBE (Figure S2b) exhibited at 362 nm. The UV-Vis absorption spectra revealed that the maximum absorbance for MeLE-ZnONPs (Figure S2c) was at 280 nm and for MeBE-ZnONPs (Figure S2d) was at 282 nm. Further, the band gap of MeLE-ZnONPs and MeBE-ZnONPs are 3.4 eV (Figure S3a) and 4.2 eV respectively (Figure S3b) indicating the formation of ZnONPs. Figure S4 shows the size distribution of ZnONPs in both MeLE (Figure S4a) and MeBE (Figure S4b) analyzed through DLS.

The IR spectra of the synthesized MeLE-ZnONPs have been depicted in Figure S5a. Absorption bands at 3408 cm^{-1}, 1580 cm^{-1}, 1502 cm^{-1}, 1380 cm^{-1}, 1377 cm^{-1}, 1046 cm^{-1}, 935 cm^{-1}, 834 cm^{-1}, 673 $cm^{-1}$and 417 cm^{-1} were observed. Figure S5b displays the IR spectra of the synthesized MeBE-ZnONPs indicating the broad and strong absorption bands at 3409 cm^{-1}, 1578 cm^{-1}, 1384 cm^{-1}, 1488 cm^{-1}, 1331 cm^{-1}, 1032 cm^{-1}, 942 cm^{-1}, 830 cm^{-1}, 666 cm^{-1} and 456 cm^{-1}.

The crystalline nature of the green synthesized MeLE-ZnONPs and MeBE-ZnONPs was investigated using XRD analysis as illustrated in Figure 1A (a, b). Both the XRD spectra of MeLE-ZnONPs and MeBE-ZnONPs exhibited sharp intense diffraction peaks (2θ) at 31.96°, 34.61°, 36.88°, 47.71°, 56.73°, 62.94°, 66.47°, 68.06°, 69.31°, 72.68°, 77.10°, 81.52° & 89.66° and 31.96°, 34.43°, 36.38°, 47.54°, 56.73°, 62.12°, 66.47°, 68.06°, 69.39°, 72.68°, 77.10°, 81.52° & 89.93° respectively. The zeta potential (ξ) was found to be -4.34 mV and -9.63 mV corresponding to MeLE-ZnONPs and MeBE-ZnONPs respectively. Normally, NPs in colloidal solution are said to be stable when ξ is ± 30 mV, further ξ ± 40 mV denotes good stability. The percentage yield of prepared NPs was calculated and found to be 67.3% and 76.9% for MeLE and MeBE respectively.

The surface morphology of the bulk green synthesized ZnONPs was characterized using SEM analysis. Figure S6a and Figure S6b reveal the spherically agglomerated pattern of green synthesized MeLE-ZnONPs and MeBE-ZnONPs.

Double-phase separation of synthesized NPs

The separation of MeLE-ZnONPs was accomplished by mixing an organic solvent, chloroform which is hydrophobic to the NPs dispersed in water. The TEM images of the chloroform phase and water phase ZnONPs are shown in Figure 2. The separated ZnONPs are low agglomeration and uniform spherical shape NPs. The TEM figure demonstrated a spherical shape in the chloroform phase with particle sizes ranging <50 nm whereas the water phase distribution of ZnONPs had particle sizes ranging between 50-100nm, which was further confirmed using DLS.

Anticancer activity

Figure 3 represents the cytotoxic effect of <50 nm and 50-100 nm ZnONPs against MOLT 3 cells by MTT assay. From the *in vitro* experiments, the cytotoxicity levels

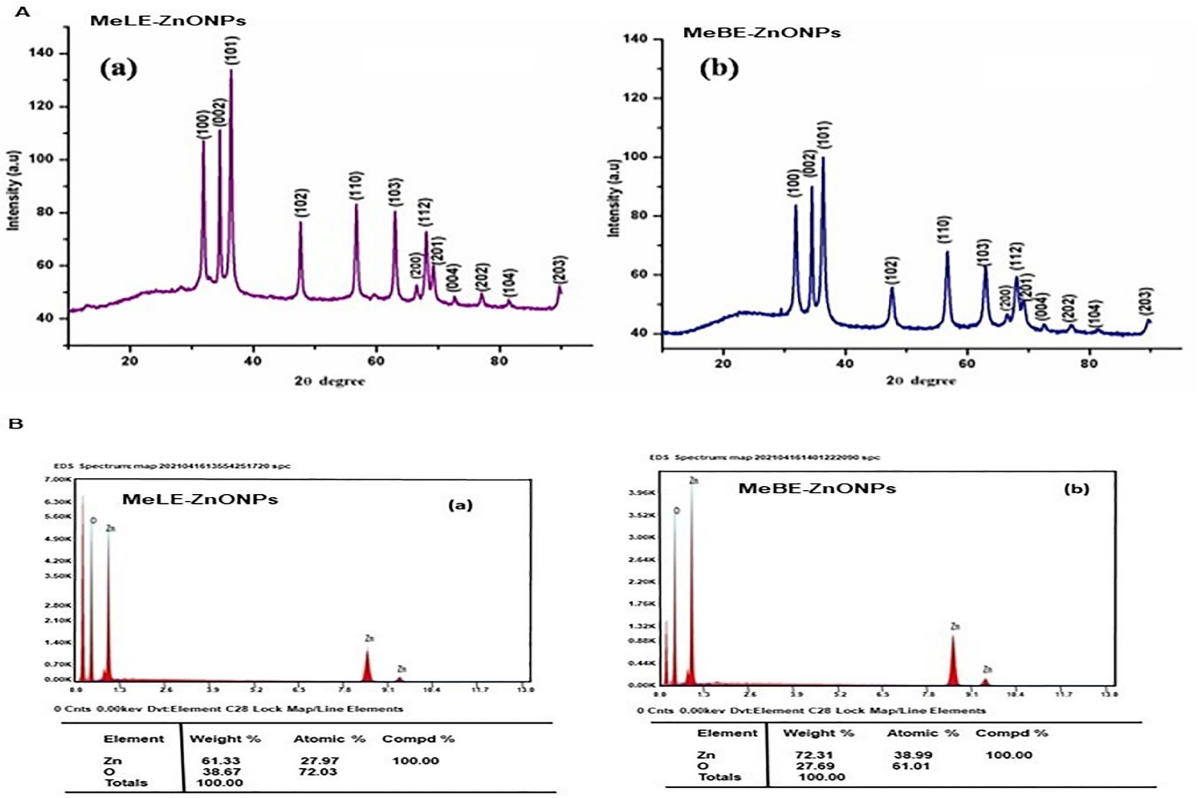

Figure 1. Fig. 1A XRD spectra of nanoparticles (Aa) MeLE-ZnONPs and (Ab) MeBE-ZnONPs.Fig. 1B. EDX mapping image of nanoparticles (Ba) MeLE-ZnONPs and (Bb) MeBE-ZnONPs.

of ZnONPs were takenafter 48 hours of incubation with different concentrations of <50 nm and 50-100 nm ZnONPs ranging from 5 to 160 µg/mL. ZnONPs of <50 nm showed statistically significant inhibition of cell growth at 10 µg/mL ($P \leq 0.05$) whereas, ZnONPs of size 50-100 nm showed inhibition of cell growth ~40 µg/mL concentrations. The IC_{50} of <50 nm ZnONPs and 50-100 nm ZnONPs were found to be ~75 µg/mL and ~102 µg/mL, respectively.

In the current investigation, AO/EtBr staining displayed a higher number of apoptotic cells on treatment with <50 nm and 50-100 nm ZnONPs compared with control (Figure 4 A-C). JC-1 staining assay showed that both the sizes of the NPs could decrease MMP, however, this decrease is more in <50 nm treated cells than that of 50-100 nm (Figure 4 D-F). The effect of autophagy can be seen in Figure 4 G-I, which is higher in 50-100 nm than that of <50 nm treated cells. In Figure 5, it can be observed that treatment with ZnONPs induces DNA damage (Figure 5 A-C), decreases cell proliferation marker ki 67 (Figure 5 D-F), and increases oxidative stress (Figure 5 G-I) when compared to control cells. Here, we did not observe any statistically significant difference between the two different sizes of IC_{50} dose of ZnONPs treated cells.

Discussion

Our earlier reports reveal the leaf extract of *D. montana* possesses various phytoconstituents[27] including flavonoids, terpenoids, phenols, tannins, etc., The bark extract studied currently also shows the presence of alkaloids, steroids, phenols, terpenoids, flavonoids, and tannins.[43] These phytochemicals present in the natural resource could facilitate nanoparticle formation by its inherited characteristics such as reducing/oxidizing etc. Further, NPs synthesized through plant extract are value-added and may be stable at a neutral solution because of the capping property of active principles present in it. Inaddition, bioactive constituents present in the plant extracts are proficient at multi-functioning which makes them the most suitable candidate for anticancer drug development.[44] Hence, MeLE and MeBE were used for the efficient synthesis of ZnONPs. Bioactive constituents namely phenolic, tannins, and flavonoids present in MeLE and MeBE act as reducing and stabilizing agents, by the presence of OH groups, for NPs formation.[45,46] Most of the active bio-constituents do not possess adverse effects *in vivo*. Further, it is reported that they efficiently reduce the metal ions and produce NPs of different shapes, sizes, and dimensions.[47]

The IR spectra of the synthesized MeLE-ZnONPs show a wide band at 3408 cm^{-1} corresponding to O-H stretch, H-bonded. The strong band at 1580 cm^{-1} is due to N-H bend in alkenes. The small band was noticed at 1502 cm^{-1} confirming C-C stretch due to (in-ring) aromatics. The sharp and small bands obtained at 1380

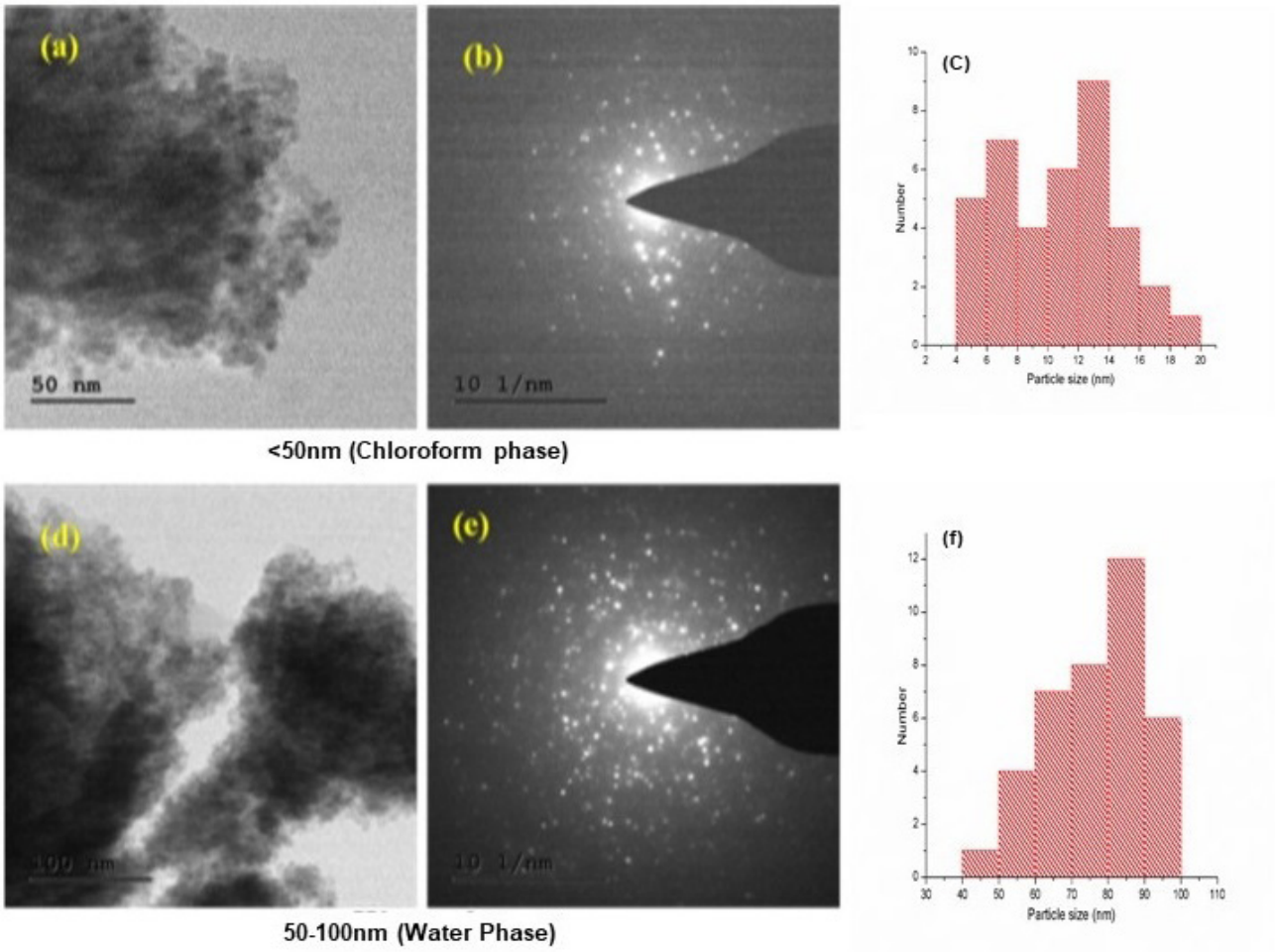

Figure 2. (a) TEM image of ZnONPs in chloroform phase (<50 nm), (b) selected area electron diffraction patterns of ZnONPs in chloroform phase, (c) particle size distribution of ZnONPs in chloroform phase using DLS, (d) TEM image of ZnONPs in water phase (50-100 nm), (e) selected area electron diffraction patterns of ZnONPs in water phase and (f) particle size distribution of ZnONPs in water phase using DLS.

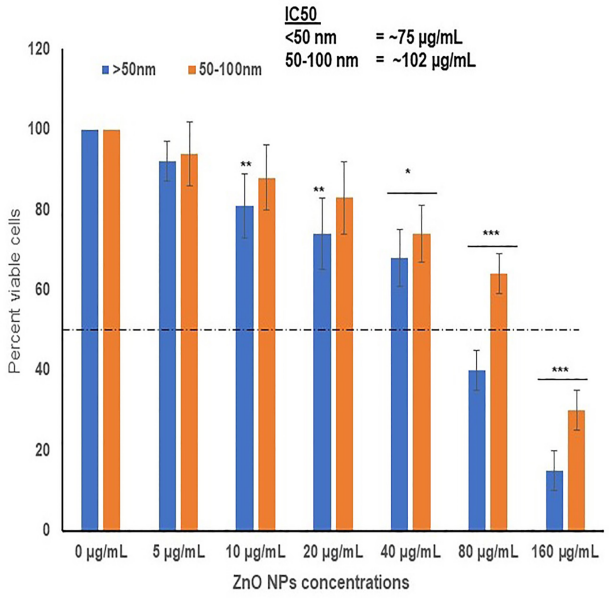

Figure 3. Cell viability through MTT assay of ZnONPs at <50 nm size and 50-100nm size. Statistical analysis, ANOVA, and Tukey's multiple tests were used. *p<0.05, **p<0.01, ***p<0.001 Vs control.

cm^{-1}, and 1377 cm^{-1} show the N-O and -CH_3 stretching bonds. The medium absorption bands that occur in the region of 1046 cm^{-1}, 935 cm^{-1}, and 834 cm^{-1}, were attributed to the wagging of C-O stretch, O-H bend, and C-Cl in alcohol, acids, and alkyl halides. The prominent sharp peak at 673 cm^{-1} and 417 cm^{-1} confirms the presence of Zn-O vibration in the synthesized green ZnONPs which is the characteristic of Zn-O bond formation. The IR spectra of the synthesized MeBE-ZnONPs display (Figure S5b) broad and strong absorption bands at 3409 cm^{-1} could be ascribed to O-H stretch, H-bonded in alcohol and phenol group. The peak at 1578 cm^{-1} corresponds to the N-H bend in alkenes and 1384 cm^{-1} attributes to SO_2 in sulphur compounds. The strong peak at 1488 cm^{-1} and 1331 cm^{-1} responds to the N-O asymmetric and symmetric stretching vibration of nitro compounds. The bands were found to be the region 1032 cm^{-1}, and 942 cm^{-1}, which causes C-O stretching of alcohol, acids, and esters. The medium absorption peak of 830 cm^{-1} is the result of C-Cl stretching vibration (alkyl halides). The medium sharp peak observed at 666 cm^{-1} and 456 cm^{-1} confirms the occurrence of Zn-O vibration in the synthesized green ZnONPs which is the characteristic of Zn-O bond

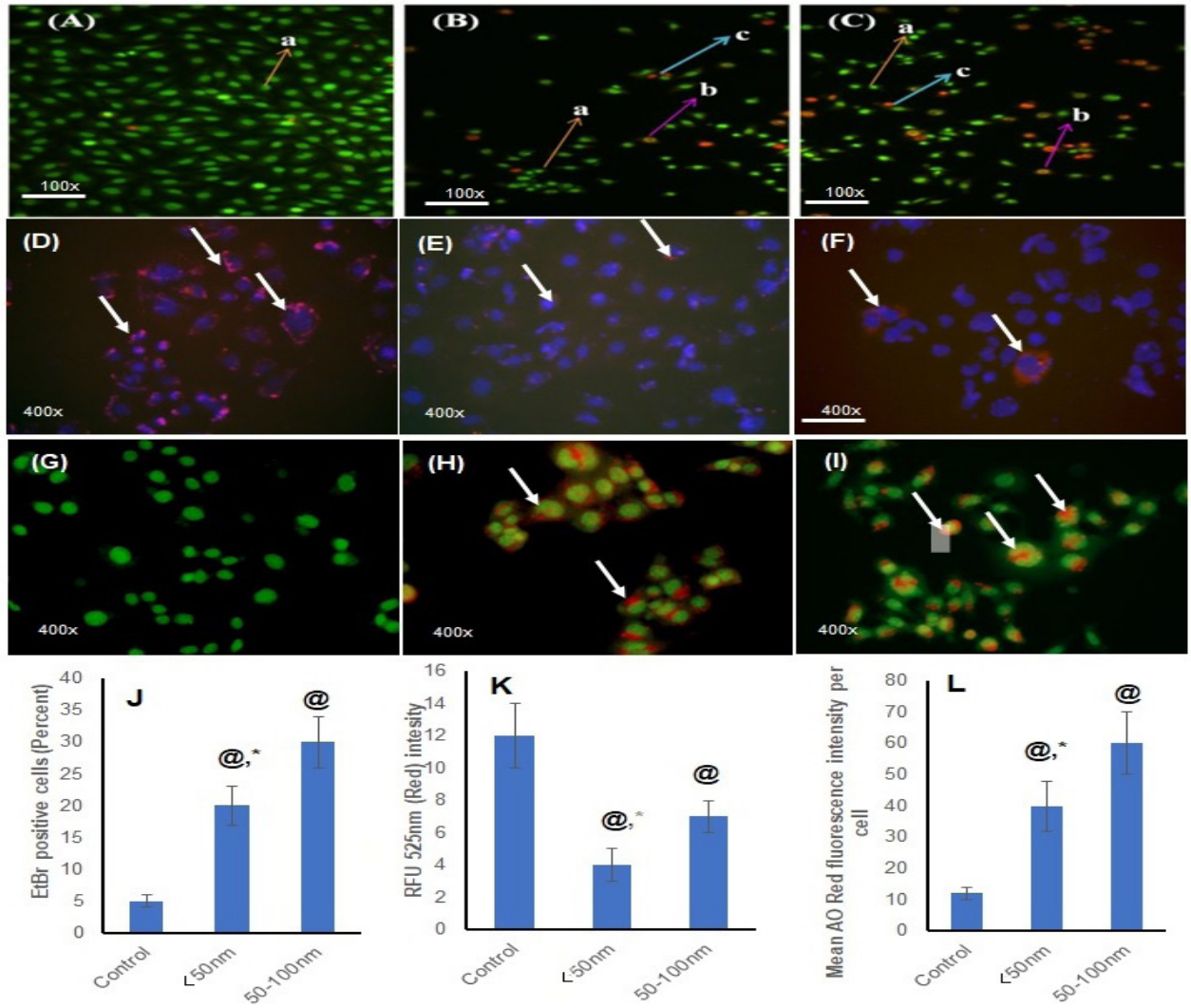

Figure 4. Different sizes of ZnONPs treated with IC_{50} concentration. Images show the AO/EtBr staining (A-C, and J), mitochondrial membrane potential (D-F, and K), and Autophagy (G-I, and L) through acidic vesicular organelles (AVO)of control and ZnONPs treated cells. (A, D, andG)-MOLT-3 cells without treatment, (B, E & H)- Treated with <50 nm ZnONPs and (C, F&I)- Exposed 50-100nm ZnONPs. Arrow mark (→) represents 'a'-live (Orange), 'b'-apoptotic (Pink),and 'c'-necrotic cells. D-I White arrow shows the positive cells (MMP or AVO). J, K, and L represent the bar diagram of respective experiments. 'a' Vs control; 'b' Vs ZnONPs treated 50-100 nm. @p<0.001, *p<0.05.

formation. The results infer that the alcohols, phenols, alkenes, carboxylic acids, esters, and aldehydes were bound to the surfaceof ZnONPs enhancing the stabilization of the NPs.[48] This study concludes that the secondary metabolites (Phenolic and flavonoid compounds) could be attributed to twin processes such as synthesis and stabilization of the NPs. Both the MeLE-ZnONPs and MeBE-ZnONPs diffraction peaks correspond to the diffraction planes of (100), (002), (101), (102), (110), (103), (200), (112), (201), (004), (202), (106) and (203). The reflection lines of MeLE-ZnONPs and MeBE-ZnONPs indicated the hexagonal phase. The diffraction planes were in good agreement with the JCPDS card no. 36- 1451 and strong narrow diffraction peaks indicated that the ZnONPs are well-crystalline structured particles.[29] Scherrer formula $D = 0.9\ \lambda/\beta \cos\theta$, (where λ is the wavelength of X-ray source (Cu Kαline – 0.1541 nm), β is the full width at half maximum in radians and θ is Bragg's diffraction angle) was used to determine the average particle size (D) of synthesized NPs. The D values of MeLE-ZnONPs and MeBE-ZnONPs were found to be 35 nm to 61 nm. Polarity and electrostatic attraction of the ZnO NPs may be attributed to its agglomeration. EDX spectra of MeLE-ZnONPs and MeBE-ZnONPs show the presence of peaks between 1kV and 10kV conforming to the presence of Zn and O as depicted in Figure 1B (a,b). These elements are present in a stoichiometric ratio which indicates there are no impurities in synthesized materials. The ZnONPs were efficiently synthesized from both MeLE and MeBE. They were characterized by sophisticated analytical tools and we found the results of MeLE and MeBE showed almost similar intensity of phytochemicals, formation of NPs, crystalline nature, shape, and purity of the nanoparticle synthesized. Hence, the MeLE was randomly chosen and

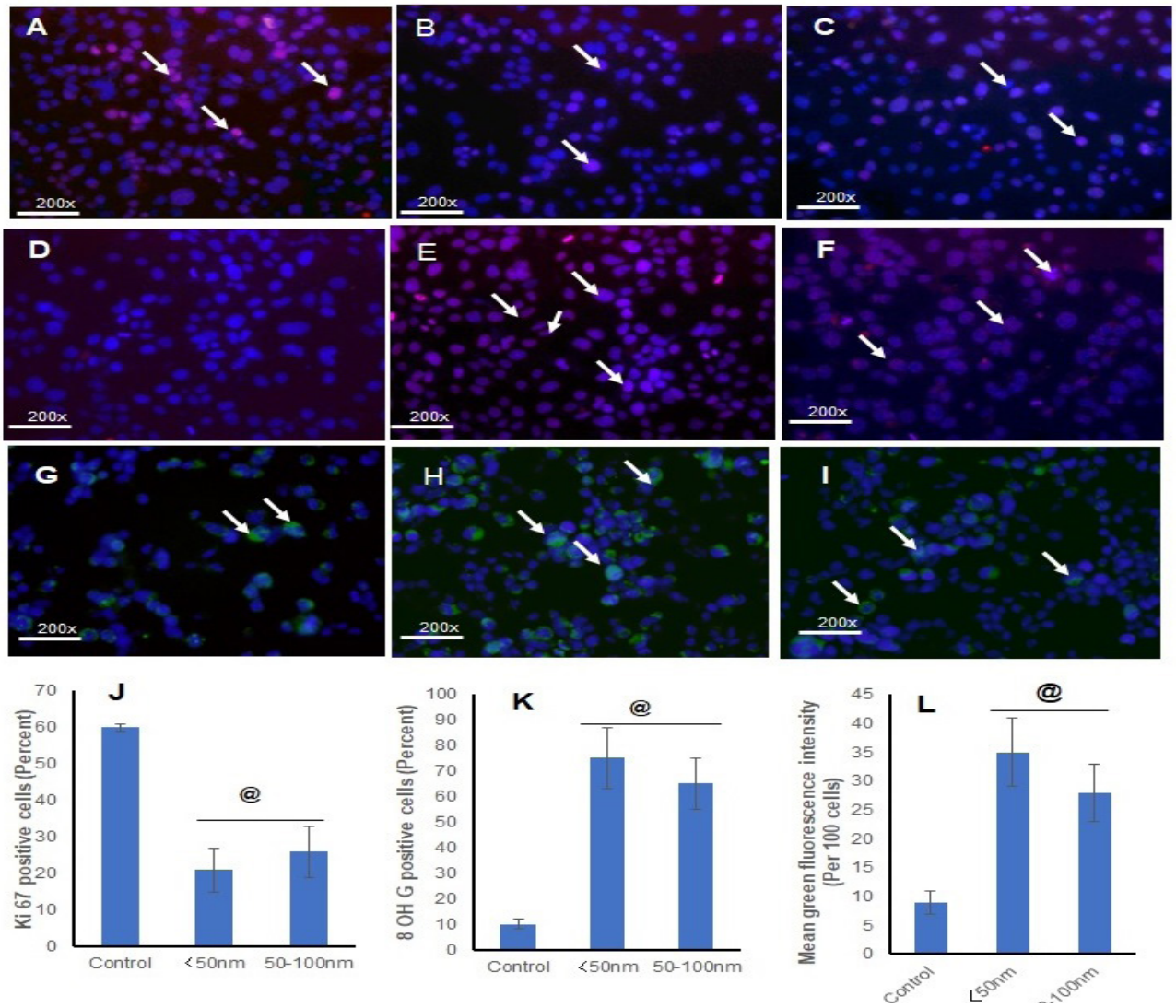

Figure 5. Different sizes of ZnONPs treated with IC_{50} concentration. Pictures show the ki67 (A-C, and J), 8-OHG (D-F, and K), and oxidative stress (G-I, and L) of control and ZnONPs treatedcells. (A, D, and G)-MOLT-3 cells without treatment, (B, E & H)- Treated with <50nm ZnONPsand (C, F&I)- Exposed 50-100nm ZnONPs. D-I White arrow shows the ki67,8-OHG and oxidative stress-positive cells. J, K, and L represent the bar diagram of respective experiments. 'a' Vs control; 'b' Vs ZnONPs treated 50-100 nm. $^{@}p<0.001$; ^{NS}-Not statistically significant.

subjected to size-separation of ZnONPs based on the double phase separation method followed by the TEM and DLS analysis to confirm the size of the separated ZnONPs. The double-phase separation method is used to separate different sizes of NPs. It is a physical phenomenon in which the particles are transported between two immiscible solvents. The phase transfer allows NPs to be dispersed in both hydrophobic and hydrophilic solvents, where both the physical and chemical properties are maintained as in the original NPs.[49] Phase transfer plays an important role in facilitating reactions where the reactants exist in two immiscible phases, such as when NPs are to be enclosed in an organic matrix as in the case of applications involving molecular electronics, etc. Phase transfer of NPs in biphasic water/organic systems has been practiced in NP synthesis to achieve controlled sizes, defined morphologies, and desired surface functionalities, where the advantages offered by aqueous and organic media are unified.[50] For example, magnetic NPs synthesized by nonpolar organic liquids have better-controlled sizes and size distributions.[51] Another study, conducted by Wei *et al.*,[52] demonstrated that the phase transfer of gold NPs of different sizes and shapes from an aqueous to organic solution can be accomplished using an ionic liquid medium.[53] This method facilitates the transfer of NPs maintaining chemical and physical properties. Preserving the size, shape, and chemical properties of the NPs is of utmost importance as they reflect their efficiency in application-oriented studies. Based on this, we used chloroform water to separate different sizes of NPs. We obtained low-ranging NPs in the chloroform phase and 50-100nm size of NPs dispersed in the water phase.

From Figure 3 it can be seen that as the concentration increases, the cytotoxicity increases, and the percent

viability decreases demonstrating a dose-dependent relationship. Both sizes of ZnONPs exhibited significant anticancer activity in MOLT-3 cells, particularly, <50nm NPs exhibited potent anticancer activity. Our findings coincide with Xu *et al.*[54] who also reported the potent anti-cancer activity of ZnONPs on the MOLT-4 cell line. On the other hand, the higher IC_{50} of 50-100 nm NPs could be due to increased size, which may be due to the decreased diffusion in the plasma membrane of the cells.[55] Recent findings reported the IC_{50} values at 175 µg/mL in HepG2 cells,[56] 121 µg/mL for MCF-7cells.[57] The present study portrays that the spherical-shaped ZnONPs of <50 nm size show ~75 µg/mL and ZnONPs of 50-100 nm size show ~102µg/mL IC_{50} values. This suggests that the greenly synthesized separated spherical ZnONPs may have the potential anticancer effect against T-ALL.To understand further the mode of action of cell death, we have used IC_{50} concentration of ZnONPs for both sizes. AO/EtBr staining showed a higher number of apoptotic cells on treatment with <50 nm and 50-100 nm ZnONPs compared with control. The results show that control cells are viable and uptake the AO whereas, the cells treated with NPs uptake the dye EtBr and appear red-orange with an an indication of cell death.[38] The study showed that treatment of ZnONPs produced dose-dependent cytotoxicity, and apoptotic morphological changes indicating that <50 nm ZnONPs show obvious advantages over 50-100 nm ZnONPs in MOLT 3 human cell lines as depicted in Figure 4 (A-C). As seen from the JC-1 staining assay (Figure 4 D-F) the decrease in MMP was more in <50nm treated cells than that of 50-100nm. Further, we tested its autophagy effect which was higher in the 50-100 nm NPs than that of <50 nm NPs treated cells. These results infer that different modes of cell death occur in ZnONPs of two different sizes. This difference could be due to the different sizes and morphologies of the NPs.[56] Literature shows that NPs with different morphologies have different physical and chemical properties.[57] We propose that the MMP alteration and autophagy-dependent pathway may be one of the mechanisms of ZnONPs-induced cell death. The results of the previous experiment show that IC_{50} concentrations of two different-sized ZnONPs, have different modes of cell death. Following this, we intended to test the DNA damage, cell proliferation, and oxidative stress markers in the cells. From Figure 5, it was found that treatment with ZnONPs induces DNA damage, decreases cell proliferation, and increases oxidative stress. These findings agree with Sharma *et al.*[58] Ezhuthupurkkal *et al.*[38] in Huh7 and HepG2 cells respectively. Similar findings were also reported by Yin *et al.*[59] in THP-1 cells, Zhao *et al.*[60] in zebrafish embryos. To our knowledge, there are no reports on any cancer cells; different sizes of ZnONPs were tested and compared to elucidate their mechanism of action. All the findings confirm that phyto-mediated ZnONPs have excellent anti-leukemia effects against T-ALL.

Conclusion

MeLE and MeBE act as an efficient reducing agent to develop ZnONPs as evidenced by UV-Vis spectra and FTIR analysis. XRD patterns and SEM analysis of both NPs reveal a crystalline nature with a hexagonal phase structure and spherical shape of NPs. EDX spectra show Zn and O elements are presented in both synthesized materials (MeLE-ZnONPs and MeBE-ZnONPs). Hence, MeLE-ZnONPs alone were separated based on their size and confirmed through TEM micrographs and DLS. Anticancer activity results demonstrated a size-dependent effect on MOLT-3 cells, as <50 nm ZnONPs show better activity than that of 50-100 nm ZnONPs. Lower particle sizes have a better anticancer effect as observed through low IC_{50} than that of higher particle NPs tested in this study. As noticed through the MMP and autophagy assays, these sizes take different routes but end at the same point as observed in DNA damage, cell proliferation, and oxidative stress markers. In future studies, the safety of the synthesized ZnONPs should be taken into consideration *in vivo*, as the passage of those NPs through normal cells could potentially influence cell apoptosis, oxidative stress, and DNA damage. In a nutshell, these results suggest that the ZnONPs of <50 nm size would contribute a vital role in treating T-ALL cancer, warranting pre-clinical practices.

Author Contributions

Sujatha Venugopal: Conceptualization, Methodology, Writing - Review & Editing. Venkatesan Alagesan: Investigation, Formal Analysis. Sancharan Acharya: Writing - Review & Editing. Thirunavukkarasu Chinnasamy: Investigation, Writing - Review & Editing.

Acknowledgements

The author VS acknowledges DST in the form of DST-KIRAN/Mobility/Sujatha/2019 for the financial support rendered. STIC, Cochin University of Science and Technology, Cochin, India; CIF- Pondicherry University, Puducherry, India are acknowledged for the characterization studies. We also acknowledge Prof. V. Dharuman, Molecular Electronics Laboratory, Department of Bioelectronics and Biosensors, School of Life Sciences, Alagappa University, Karaikudi - 630 003, India for extending his help in analyzing zeta potential.

Conflict of Interest

There are no conflicts to declare.

Supplementary Data

Supplementary data (Figures S1-S6) are available at https://doi.org/10.34172/PS.2024.4.

References

1. Teachey DT, O'Connor D. How I treat newly diagnosed T-cell acute lymphoblastic leukemia and T-cell lymphoblastic lymphoma in children. Blood. 2020;135(3):159-66. doi:10.1182/blood.2019001557

2. Kothari R, Szepietowski JC, Bagot M, Sandhu S, Patil A, Grabbe S, et al. Mycosis fungoides in pediatric population: comprehensive review on epidemiology, clinical presentation, and management. Int J Dermatol. 2022;61(12):1458-66. doi:10.1111/ijd.16098
3. Chiarini F, Lonetti A, Evangelisti C, Buontempo F, Orsini E, Evangelisti C, et al. Advances in understanding the acute lymphoblastic leukemia bone marrow microenvironment: From biology to therapeutic targeting. Biochim Biophys Acta. 2016;1863(3):449-63. doi:10.1016/j.bbamcr.2015.08.015
4. van den Brink M, Uhrberg M, Jahn L, DiPersio JF, Pulsipher MA. Selected biological issues affecting relapse after stem cell transplantation: role of T-cell impairment, NK cells and intrinsic tumor resistance. Bone Marrow Transplant. 2018;53(8):949-59. doi:10.1038/s41409-017-0078-0
5. Tomasik J, Jasiński M, Basak GW. Next generations of CAR-T cells - new therapeutic opportunities in hematology? Front Immunol. 2022;13:1034707. doi:10.3389/fimmu.2022.1034707
6. Candoni A, Lazzarotto D, Petruzzellis G. Safety of nelarabine in adults with relapsed or refractory T-cell acute lymphoblastic leukemia/lymphoma. Expert Opin Drug Saf. 2021;20(7):751-6. doi:10.1080/14740338.2021.1919621
7. Boissel N, Baruchel A. Acute lymphoblastic leukemia in adolescent and young adults: treat as adults or as children? Blood. 2018;132(4):351-61. doi:10.1182/blood-2018-02-778530
8. 8. You MJ, Medeiros LJ, Hsi ED. T-lymphoblastic leukemia/lymphoma. Am J Clin Pathol. 2015;144(3):411-22. doi:10.1309/AJCPMF03LVSBLHPJ
9. Jain N, Lamb AV, O'Brien S, Ravandi F, Konopleva M, Jabbour E, et al. Early T-cell precursor acute lymphoblastic leukemia/lymphoma (ETP-ALL/LBL) in adolescents and adults: a high-risk subtype. Blood. 2016;127(15):1863-9. doi:10.1182/blood-2015-08-661702
10. Siegel RL, Miller KD, Jemal A. Cancer statistics, 2019. CA Cancer J Clin. 2019;69(1):7-34. doi:10.3322/caac.21551
11. Zhang J, Ding L, Holmfeldt L, Wu G, Heatley SL, Payne-Turner D, et al. The genetic basis of early T-cell precursor acute lymphoblastic leukaemia. Nature. 2012;481(7380):157-63. doi:10.1038/nature10725
12. Stock W, Luger SM, Advani AS, Yin J, Harvey RC, Mullighan CG, et al. A pediatric regimen for older adolescents and young adults with acute lymphoblastic leukemia: results of CALGB 10403. Blood. 2019;133(14):1548-59. doi:10.1182/blood-2018-10-881961
13. Przespolewski A, Szeles A, Wang ES. Advances in immunotherapy for acute myeloid leukemia. Future Oncol Lond Engl. 2018;14(10):963-78. doi:10.2217/fon-2017-0459
14. Alimardani V, Rahiminezhad Z, DehghanKhold M, Farahavar G, Jafari M, Abedi M, et al. Nanotechnology-based cell-mediated delivery systems for cancer therapy and diagnosis. Drug Deliv Transl Res. 2023;13(1):189-221. doi:10.1007/s13346-022-01211-9
15. Shao C, Li Z, Zhang C, Zhang W, He R, Xu J, et al. Optical diagnostic imaging and therapy for thyroid cancer. Mater Today Bio. 2022;17:100441. doi:10.1016/j.mtbio.2022.100441
16. Zhang C, Zhao J, Wang W, Geng H, Wang Y, Gao B. Current advances in the application of nanomedicine in bladder cancer. Biomed Pharmacother. 2023;157:114062. doi:10.1016/j.biopha.2022.114062
17. Karmous I, Pandey A, Haj KB, Chaoui A. Efficiency of the green synthesized nanoparticles as new tools in cancer therapy: insights on plant-based bioengineered nanoparticles, biophysical properties, and anticancer roles. Biol Trace Elem Res. 2020;196(1):330-42. doi:10.1007/s12011-019-01895-0
18. Adeyemi JO, Oriola AO, Onwudiwe DC, Oyedeji AO. Plant extracts mediated metal-based nanoparticles: synthesis and biological applications. Biomolecules. 2022;12(5):627. doi:10.3390/biom12050627
19. Naiel B, Fawzy M, Halmy MWA, Mahmoud AED. Green synthesis of zinc oxide nanoparticles using Sea Lavender (*Limonium pruinosum* L. Chaz.) extract: characterization, evaluation of anti-skin cancer, antimicrobial and antioxidant potentials. Sci Rep. 2022;12(1):20370. doi:10.1038/s41598-022-24805-2
20. Sahoo A, Jena AK, Panda M. Experimental and clinical trial investigations of phyto-extracts, phyto-chemicals and phyto-formulations against oral lichen planus: A systematic review. J Ethnopharmacol. 2022;298:115591. doi:10.1016/j.jep.2022.115591
21. Singh S, Sharma B, Kanwar SS, Kumar A. Lead Phytochemicals for Anticancer Drug Development. Front Plant Sci. 2016;7:1667. doi:10.3389/fpls.2016.01667
22. Truchado DA, Rincón S, Zurita L, Sánchez F, Ponz F. Isopeptide bonding in planta allows functionalization of elongated flexuous proteinaceous viral nanoparticles, including non-viable constructs by other means. Viruses. 2023;15(2):375. doi:10.3390/v15020375
23. Ovais M, Khalil AT, Raza A, Khan MA, Ahmad I, Islam NU, et al. Green synthesis of silver nanoparticles via plant extracts: beginning a new era in cancer theranostics. Nanomed. 2016;11(23):3157-77. doi:10.2217/nnm-2016-0279
24. Ravishankara MN, Shrivastava N, Jayathirtha MG, Padh H, Rajani M. Sensitive high-performance thin-layer chromatographic method for the estimation of diospyrin, a tumour inhibitory agent from the stem bark of Diospyros montana Roxb. J Chromatogr B Biomed Sci App. 2000;744(2):257-62. doi:10.1016/s0378-4347(00)00277-2
25. Das Sarma M, Ghosh R, Patra A, Hazra B. Synthesis

of novel aminoquinonoid analogues of diospyrin and evaluation of their inhibitory activity against murine and human cancer cells. Eur J Med Chem. 2008;43(9):1878-88. doi:10.1016/j.ejmech.2007.11.028
26. Kantamreddi VSS, Wright CW. Investigation of Indian diospyros species for antiplasmodial properties. Evid-Based Complement Altern Med. 2008;5(2):187-90. doi:10.1093/ecam/nem019
27. Kokila K, Elavarasan N, Sujatha V. *Diospyros montana* leaf extract-mediated synthesis of selenium nanoparticles and their biological applications. New J Chem. 2017;41(15):7481-90. doi: 10.1039/C7NJ01124E
28. Khan MT, Azhar I, Shehzadi N, Hussain K, Parveen S, Hanif U. Morphological, microscopic, and physicochemical studies of *Diospyros montana*. Microsc Res Tech. 2020;83(10):1260-81. doi:10.1002/jemt.23520
29. Bharathi D, Diviya Josebin M, Vasantharaj S, Bhuvaneshwari V. Biosynthesis of silver nanoparticles using stem bark extracts of *Diospyros montana* and their antioxidant and antibacterial activities. J Nanostructure Chem. 2018;8(1):83-92. doi:10.1007/s40097-018-0256-7
30. Islam F, Shohag S, Uddin MJ, Islam MR, Nafady MH, Akter A, et al. Exploring the journey of zinc oxide nanoparticles (ZnO-NPs) toward biomedical applications. Mater Basel Switz. 2022;15(6):2160. doi:10.3390/ma15062160
31. Senthilkumar SR, Thirumal S. Green tea (*Camellia sinensis*) mediated synthesis of zinc oxide (ZnO) nanoparticles and studies on their antimicrobial activities. Int J Pharm Pharm Sci. 2014;6:461-5.
32. Cavalu S, Antoniac IV, Mohan A, Bodog F, Doicin C, Mates I, et al. Nanoparticles and nanostructured surface fabrication for innovative cranial and maxillofacial surgery. Mater Basel Switz. 2020;13(23):5391. doi:10.3390/ma13235391
33. Taccola L, Raffa V, Riggio C, Vittorio O, Iorio MC, Vanacore R, et al. Zinc oxide nanoparticles as selective killers of proliferating cells. Int J Nanomedicine. 2011;6:1129-40. doi:10.2147/IJN.S16581
34. Akhtar MJ, Ahamed M, Kumar S, Khan MM, Ahmad J, Alrokayan SA. Zinc oxide nanoparticles selectively induce apoptosis in human cancer cells through reactive oxygen species. Int J Nanomedicine. 2012;7:845-57. doi:10.2147/IJN.S29129
35. Premanathan M, Karthikeyan K, Jeyasubramanian K, Manivannan G. Selective toxicity of ZnO nanoparticles toward Gram-positive bacteria and cancer cells by apoptosis through lipid peroxidation. Nanomedicine Nanotechnol Biol Med. 2011;7(2):184-92. doi:10.1016/j.nano.2010.10.001
36. Hou D, Xie C, Huang K, Zhu C. The production and characteristics of solid lipid nanoparticles (SLNs). Biomaterials. 2003;24(10):1781-5. doi:10.1016/s0142-9612(02)00578-1
37. Qian F, Lan PC, Olson T, Zhu C, Duoss EB, Spadaccini CM, et al. Multiphase separation of copper nanowires. Chem Commun. 2016;52(78):11627-30. doi:10.1039/c6cc06228h
38. Ezhuthupurakkal PB, Ariraman S, Arumugam S, Subramaniyan N, Muthuvel SK, Kumpati P, et al. Anticancer potential of ZnO nanoparticle-ferulic acid conjugate on Huh-7 and HepG2 cells and diethyl nitrosamine induced hepatocellular cancer on Wistar albino rat. Nanomedicine Nanotechnol Biol Med. 2018;14(2):415-28. doi:10.1016/j.nano.2017.11.003
39. Venkateasan A, Prabakaran R, Sujatha V. Phytoextract-mediated synthesis of zinc oxide nanoparticles using aqueous leaves extract of Ipomoea pes-caprae (L).R.br revealing its biological properties and photocatalytic activity. Nanotechnol Environ Eng. 2017;2(1):8. doi:10.1007/s41204-017-0018-7
40. Smiley ST, Reers M, Mottola-Hartshorn C, Lin M, Chen A, Smith TW, et al. Intracellular heterogeneity in mitochondrial membrane potentials revealed by a J-aggregate-forming lipophilic cation JC-1. Proc Natl Acad Sci U S A. 1991;88(9):3671-5. doi:10.1073/pnas.88.9.3671
41. Damas-Souza DM, Nunes R, Carvalho HF. An improved acridine orange staining of DNA/RNA. Acta Histochem. 2019;121(4):450-4. doi:10.1016/j.acthis.2019.03.010
42. Wojtala A, Bonora M, Malinska D, Pinton P, Duszynski J, Wieckowski MR. Methods to monitor ROS production by fluorescence microscopy and fluorometry. Methods Enzymol. 2014;542:243-62. doi:10.1016/B978-0-12-416618-9.00013-3
43. Sujatha V, Kaviyasri G, Venkatesan A, Thirunavukkarasu C, Acharya S, Bin Dayel S, et al. Biomimetic formation of silver oxide nanoparticles through *Diospyros montana* bark extract: Its application in dye degradation, antibacterial and anticancer effect in human hepatocellular carcinoma cells. J King Saud Univ - Sci. 2023;35(3):102563. doi:10.1016/j.jksus.2023.102563
44. Singh B, Singh JP, Kaur A, Singh N. Bioactive compounds in banana and their associated health benefits – A review. Food Chem. 2016;206:1–11. doi:10.1016/j.foodchem.2016.03.033
45. Ahmed S, Annu, Chaudhry SA, Ikram S. A review on biogenic synthesis of ZnO nanoparticles using plant extracts and microbes: A prospect towards green chemistry. J Photochem Photobiol B. 2017;166:272-84. doi:10.1016/j.jphotobiol.2016.12.011
46. Singh J, Dutta T, Kim KH, Rawat M, Samddar P, Kumar P. 'Green' synthesis of metals and their oxide nanoparticles: applications for environmental remediation. J Nanobiotechnology. 2018;16(1):84. doi:10.1186/s12951-018-0408-4
47. Sharma R, Garg R, Kumari A. A review on biogenic synthesis, applications and toxicity aspects of zinc oxide nanoparticles. EXCLI J. 2020;19:1325-40.

doi:10.17179/excli2020-2842
48. Chikkanna MM, Neelagund SE, Rajashekarappa KK. Green synthesis of Zinc oxide nanoparticles (ZnO NPs) and their biological activity. SN Appl Sci. 2018;1(1):117. doi:10.1007/s42452-018-0095-7
49. Cook E, Labiento G, Chauhan BPS. Fundamental methods for the phase transfer of nanoparticles. Molecules. 2021;26(20):6170. doi:10.3390/molecules26206170
50. Bao C, Horton JM, Bai Z, Li D, Lodge TP, Zhao B. Stimuli-triggered phase transfer of polymer-inorganic hybrid hairy particles between two immiscible liquid phases. J Polym Sci Part B Polym Phys. 2014;52(24):1600-19. doi:10.1002/polb.23552
51. Sun S, Zeng H, Robinson DB, Raoux S, Rice PM, Wang SX, et al. Monodisperse MFe2O4 (M = Fe, Co, Mn) nanoparticles. J Am Chem Soc. 2004;126(1):273-9. doi:10.1021/ja0380852
52. Wei GT, Yang Z, Lee CY, Yang HY, Wang CRC. Aqueous-organic phase transfer of gold nanoparticles and gold nanorods using an ionic liquid. J Am Chem Soc. 2004;126(16):5036–7. doi:10.1021/ja039874m
53. Soliman MG, Pelaz B, Parak WJ, del Pino P. Phase transfer and polymer coating methods toward improving the stability of metallic nanoparticles for biological applications. Chem Mater. 2015;27(3):990-7. doi:10.1021/cm5043167
54. Xu Z, Wu Y, Song L, Chinnathambi A, Ali Alharbi S, Fang L. Anticarcinogenic effect of zinc oxide nanoparticles synthesized from Rhizoma paridis saponins on Molt-4 leukemia cells. J King Saud Univ - Sci. 2020;32(3):1865-71. doi:10.1016/j.jksus.2020.01.023
55. Rückerl F, Käs JA, Selle C. Diffusion of nanoparticles in monolayers is modulated by domain size. Langmuir ACS J Surf Colloids. 2008;24(7):3365-9. doi:10.1021/la703140b
56. Guleria A, Chakraborty S, Neogy S, Maurya DK, Adhikari S. Controlling the phase and morphology of amorphous Se nanoparticles: their prolonged stabilization and anticancer efficacy. Chem Commun. 2018;54(63):8753-6. doi:10.1039/C8CC05375H
57. Castellanos-Rubio I, Arriortua O, Marcano L, Rodrigo I, Iglesias-Rojas D, Barón A, et al. Shaping up Zn-doped magnetite nanoparticles from mono- and bimetallic oleates: the impact of Zn content, Fe vacancies, and morphology on magnetic hyperthermia performance. Chem Mater. 2021;33(9):3139-54. doi:10.1021/acs.chemmater.0c04794
58. Sharma V, Anderson D, Dhawan A. Zinc oxide nanoparticles induce oxidative DNA damage and ROS-triggered mitochondria mediated apoptosis in human liver cells (HepG2). Apoptosis. 2012;17(8):852-70. doi:10.1007/s10495-012-0705-6
59. Yin X, Li Z, Lyu C, Wang Y, Ding S, Ma C, et al. Induced effect of zinc oxide nanoparticles on human acute myeloid leukemia cell apoptosis by regulating mitochondrial division. IUBMB Life. 2022;74(6):519-31. doi:10.1002/iub.2615
60. Zhao X, Ren X, Zhu R, Luo Z, Ren B. Zinc oxide nanoparticles induce oxidative DNA damage and ROS-triggered mitochondria-mediated apoptosis in zebrafish embryos. Aquat Toxicol. 2016;180:56-70. doi:10.1016/j.aquatox.2016.09.013